

Fluctuations in EEG band power over minutes to days explain how seizures change over time

Mariella Panagiotopoulou¹, Christoforos Papasavvas¹, Gabrielle M Schroeder¹, Peter Taylor^{1,2,3}, Yujiang Wang^{*1,2,3}

December 22, 2024

1. CNNP Lab (www.cnnp-lab.com), Interdisciplinary Computing and Complex BioSystems Group, School of Computing, Newcastle University, Newcastle upon Tyne, United Kingdom
2. Faculty of Medical Sciences, Newcastle University, Newcastle upon Tyne, United Kingdom
3. UCL Queen Square Institute of Neurology, Queen Square, London, United Kingdom

* Yujiang.Wang@newcastle.ac.uk

Abstract

Epilepsy is recognised as a dynamic disease, where seizures and their features change over time. Specifically, we recently demonstrated that seizures themselves change in terms of their evolution. However, the underpinning modulators of seizure evolution remain unclear.

In this work, we analyse continuous (interictal) intracranial Electroencephalographic (iEEG) recordings, and elucidate fluctuations in iEEG band power over different timescales (ranging from minutes to days).

We find that all patients show an approximately circadian fluctuation in their EEG band power, but also many other fluctuations on patient-specific timescales. Importantly, we find that a combination of fluctuations on different timescales can explain the changes in seizure evolution in most patients above chance-level.

We interpret these results as evidence that seizure modulating factors exist, and they vary over time (patient-specifically). These time-varying modulating factors can be captured in fluctuations of EEG band power, and future work should link them to the exact biological time-varying processes.

1 Introduction

Epilepsy is a common neurological condition, characterised by recurrent, unprovoked seizures [1]. It affects approximately 1% of the world’s population and a third of the patients experience refractory epilepsy, where seizures are not adequately controlled despite medication.

Importantly, epilepsy is not a static disorder; seizures and pathological brain activity have been shown to fluctuate over hours to years. In terms of the seizures, changes are observed in terms of their evolution, spread and dynamics from one seizure to the next. Clinical symptoms and severity of the seizure also correlate with the observed changes in seizure dynamics. While a subset of seizures might share common features in the same patient, our recent work [2] has shown that functional network dynamics of epileptic seizures change over time in the same patient. Notably, these changes followed daily (circadian) fluctuations in approximately a third of the patients, and longer-term fluctuations, or a mixture between the two was seen in almost all remaining patients [2]. In support of our observations, a recent study quantifying univariate properties of seizure onset and offset also noted that different types of dynamics can be seen across different seizures in the same patient [3, 4]. Thus, epileptic seizures are not a deterministic sequence of abnormal brain activity patterns, but are clearly modulated by processes, which shape the neural activity during a seizure and affect the severity of the seizure.

One hypothesis explaining these observations is that the diversity of seizures may arise from fluctuations in the underlying interictal brain states. It is well-known that spectral properties of the electroencephalogram (EEG) change in each channel from moment to moment [5]. Global and local characteristics of the interictal functional network have been demonstrated to fluctuate over the timescale of hours to days, with a strong effect of the circadian rhythm [6, 7, 8]. Interictal fluctuations related to epilepsy have also been reported. For example, high frequency oscillation (HFO) rates vary in location and power within each patient over time [9]. Interictal spikes also change in their location and rate over hours to days [10, 11]. Interestingly, periodicity in interictal spikes over long time scales (days, weeks, months) has also been shown to be associated with seizure occurrence [10, 12]. Therefore, it remains an open question if variability in seizure dynamics can be explained to some degree by temporal fluctuations of interictal brain activity on different timescales.

We seek to address this question by exploring what temporal fluctuations of interictal brain activity best explain the diversity in seizure dynamics for each individual patient. Most previous research has focused on analysing spikes, bursts, or HFOs and their association with seizure occurrence. However, an analysis of the factors driving changes in *dynamics* from one seizure to the next is missing. Additionally, we seek to explore the full range of all possible brain activity patterns, which will include epilepsy-related activity patterns (e.g. spikes), but are patient-specific. Therefore, we will analyse temporal fluctuations in wide-ranging spectral properties of long-term EEG, using with patient-specific pattern detection. We will analyse which frequency bands, or groups of channels contribute to fluctuations of particular timescales. Finally, we will explore the association of fluctuations on different timescales with seizure variability in each patient.

2 Methods

2.1 Data acquisition

For the purpose of this study, we used open source data from patients with drug-resistant epilepsy (available at <http://ieeg-swez.ethz.ch>). The data consist of a total of 2656 hours of long-term in-

Patient	Duration in hours	Duration in days	Number of Seizures	Mean seizure duration (minutes)
ID01	293	12	2	10.030
ID02	235	10	2	1.468
ID03	158	7	4	1.078
ID04	41	2	14	0.699
ID05	109	5	4	0.278
ID06	146	6	8	0.765
ID07	69	3	4	1.159
ID08	144	6	70	0.366
ID09	41	2	27	0.706
ID10	42	2	17	1.181
ID11	212	9	2	1.526
ID12	191	8	9	2.441
ID13	104	4	7	1.717
ID14	161	7	60	0.430
ID15	196	8	2	1.576
ID16	177	7	5	3.174
ID17	130	5	2	1.632
ID18	205	9	5	3.319
Total	2656	111	244	
Average				1.864

Table 1: For each subject (**Patient**) the following descriptive information is provided: **Duration in hours:** duration of iEEG recordings in hours. **Duration in days:** duration of iEEG recordings in days. **Number of Seizures:** number of patient’s seizures annotated. **Mean seizure duration:** mean duration across all seizures in minutes.

tracranial electroencephalography (iEEG) from 18 subjects. Continuous recordings in each subject cover 24 to 128 channels and vary between 2 to 12 days. Sampling frequency was either 512 or 1024 Hz depending on the subject. Electrodes (strip, grid, and depth) were implanted intracranially by clinicians. The collection of the data was conducted in the Sleep-Wake-Epilepsy-Center (SWEC) at the University Hospital of Bern, Department of Neurology, as part of their presurgical evaluation programme, independently of this study [13].

iEEG signals were provided in already pre-processed form. Briefly, signals have been median-referenced and band-pass filtered from 0.5-120 Hz using a 4th order Butterworth filter (forward and backward). Seizure onset and termination times were determined by a board-certified epileptologist. Channels with artifacts were also identified and excluded by the same epileptologist. All the steps so far were conducted independently of this study resulting to publicly available data. All patients formally consented to their iEEG data being used for research purposes[13].

2.2 IEEG preprocessing

We performed additional preprocessing steps to extract iEEG band power from the five main frequency bands (Fig. 1a). For each recording channel, the signal was divided into 3 s epochs (Fig. 1b). For each epoch, the band power was computed for the following frequency bands:

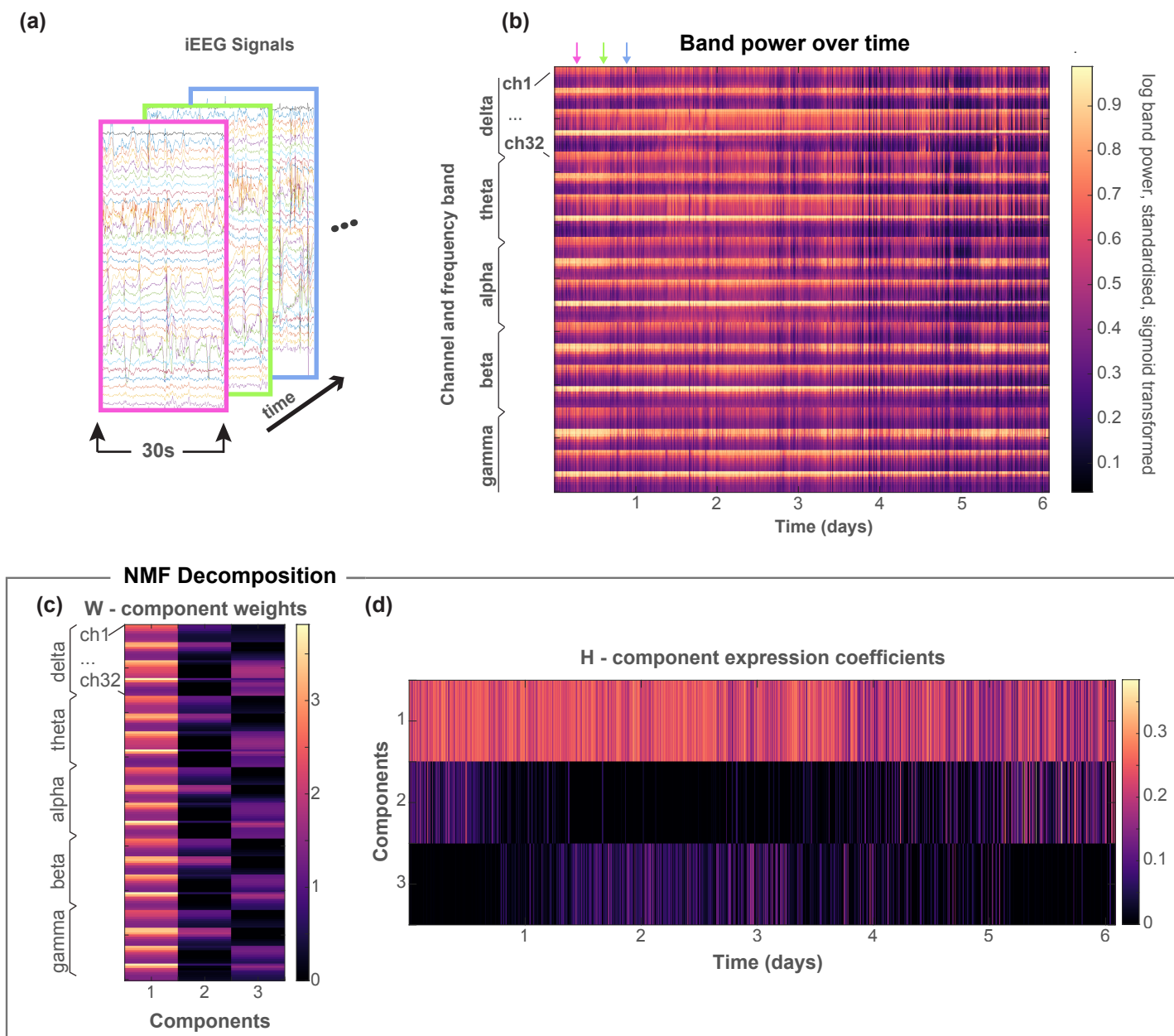


Figure 1: Workflow of data pre-processing; calculation of Band Power and NMF implementation. (a) 30 s segments were extracted along the recording from the multi-channel iEEG. The presentation of iEEG signals here is used as an example; it does not reflect 30 s recording segments. (b) The log of the standardised band power. (c)&(d) NMF is performed to the band power matrix resulting into the decomposition $W \times H$. (c) W contains the basis vectors; (d) The coefficient matrix H gives the pattern of the contribution of each basis vector to the observed values of frequency band.

δ : 1 – 4 Hz, θ : 4 – 8 Hz, α : 8 – 13 Hz, β : 13 – 30 Hz and γ : 30 – 80 Hz. The band powers were computed using Welch’s method with 1 s sliding window and an overlap of 0.5 s between consecutive windows. To ensure computational tractability, the band power was subsequently averages every 30 s (i.e. every 10 epochs) giving rise to a time series of band power that was sampling an average every 30 s. The band power values were aggregated into band-specific matrices with dimensions

$\#channels \times \#epochs$. Then, these matrices were log transformed, and standardised across all epochs and channels within a frequency band. To enable subsequent analysis steps, we also Sigmoid transformed ($S(x) = [1 + \exp(-x)]^{-1}$) the standardised data to ensure positive entries between 0 and 1. For each patient, we then concatenated the matrices from all frequency bands yielding a single $(5 \times \#channels) \times \#epochs$ (henceforth defined as $n \times T$) matrix (Fig. 1b). We will also refer to this matrix as the data matrix X throughout the paper.

2.3 Non-Negative Matrix Factorization for dimensionality reduction

As the data matrix X is high-dimensional with redundant information, we applied a dimensionality reduction step to the data. Dimensionality reduction was performed on the matrix X defined in Section 2.2 using NMF [14]. NMF approximates a non-negative input matrix $X \in \mathbb{R}_+^{n \times T}$ as the product of two non-negative matrices, $W \in \mathbb{R}_+^{n \times k}$ and $H \in \mathbb{R}_+^{k \times T}$, such that $X \approx W \times H \equiv X'$, given an integer k . Specifically, we applied the non-negative singular value decomposition (SVD) with low-rank correction (NNSVD-LRC) [15], which is an NMF algorithm based on SVD that uses in every iteration of the optimisation process the discarded SVD factors for the initialisation step.

In this way, we can decompose each subject’s band power data matrix X into W and H matrices (Fig. 1c-d). Every column of matrix W represents a single NMF component and is a basis vector or feature vector with n elements/features. Each row of H represents how a single NMF component evolves over time across all T time epochs.

To determine the optimal number of representative NMF components, k , we scanned $3 \leq k \leq 15$ in each subject. For each value of k we performed NNSVD-LRC, obtained a W and H and calculated the relative reconstruction errors $\sum_{n,T} |X - X'| / (n \times T)$. We also calculated $c = \max\{\max(|Corr(W)|), \max(|Corr(H)|)\}$ for each k , where $\max(|Corr(W)|)$ represents the max absolute correlation among all column pairs of W , and $\max(|Corr(H)|)$ represents the max absolute correlation among all row pairs of H . In simple words, we calculated the strongest correlation or anticorrelation between NMF components in terms of their feature weights W and their expression coefficient time series H . We then selected $k = 15$, or the k yielding the smallest correlation between the NMF components that has a relative reconstruction error smaller than 5%, which ever is smaller. This means that different subjects had a distinct number of NMF components, k .

2.4 Multivariate Empirical Mode Decomposition

After applying NMF with the optimal choice of k , we obtained two matrices for each subject, W and H . The matrix W consists of the basis vectors, while H is a multivariate time-series with dimensions equal to $k \times T$ (= the number of NMF components \times the total number of epochs), as already described in Section 2.3.

To investigate fluctuations in the band power data on different timescales, we analysed the matrix H using Empirical Mode Decomposition (EMD) [16, 17]. It is well known that EEG signals are non-stationary processes characterised by time-varying features [18, 19]. EMD is a data-adaptive method able to detect non-stationary and non-rhythmic fluctuations on different timescales. EMD decomposes an input signal, say $Y(t)$, into M finite narrow-band fluctuations, known as intrinsic mode functions (IMF), based on the local extrema of a time-series: $Y(t) = \sum_{i=1}^M IMF_i(t) + r(t)$, where $r(t)$ is the residue signal. This process is called sifting process [16]. For the purpose of this analysis, we used an extension of this method to the multi-dimensional space called Multivariate Empirical Mode Decomposition (MEMD) [16, 17, 20]. Therefore, the

matrix H can be represented by the sum of M multi-dimensional IMF signals (dimension for each IMF would be equal to k ; i.e. the number of rows of the matrix H /NMF components). To clarify, we can think of all IMFs in a specific dimension as the decomposition of the corresponding NMF component. If we denote $IMF_{i,j}$ the dimension j of the IMF_i signal, then the j -th NMF component $Y_j(t)$ can be written as $Y_j(t) = \sum_{i=1}^M IMF_{i,j}(t) + r_j(t)$. This equation applies to every NMF component $j = 1, \dots, k$.

We then apply a Hilbert-transform on each dimension of the IMF (following classical analysis methods for EMD) to obtain the instantaneous frequency, phase, and amplitude.

For any (real-valued) univariate signal, say $u(t)$, we can define its Hilbert transform as:

$$H(u)(t) = \frac{1}{\pi} P \int_{-\infty}^{+\infty} \frac{u(\tau)}{t - \tau} d\tau, \quad (1)$$

where P represent the Cauchy principal value for any function $u(t) \in L^P$ class [16].

The analytical signal $v(t)$ obtained from the Hilbert transform can be expressed as:

$$v(t) = u(t) + iH(u)(t) = a(t)e^{i\theta(t)}, \quad (2)$$

where

$$a(t) = \sqrt{u(t)^2 + H(u)(t)^2} \quad (3)$$

and

$$\theta(t) = \tan^{-1} \left(\frac{H(u)(t)}{u(t)} \right) \quad (4)$$

where $a(t)$ is the instantaneous amplitude and $\theta(t)$ is the instantaneous phase, respectively.

The instantaneous frequency, $f(t)$ can then be calculated as follows:

$$f(t) = \frac{d\theta(t)}{dt}. \quad (5)$$

The application of EMD along with Hilbert transform leads to the so-called Hilbert-Huang transform. Through the Hilbert spectral analysis, each IMF's instantaneous frequency can be represented as functions of time. The result is a frequency-time distribution of signal amplitude (or energy using the squared values of amplitude, $a^2(t)$), designated as Hilbert amplitude spectrum or Hilbert spectrum (or Hilbert energy spectrum if energy is used instead of amplitude), $H(f, t)$.

For each univariate IMF, we can obtain the Hilbert energy spectrum as a function of instantaneous frequency and time mathematically using the following formulas:

$$H(f, t) = \begin{cases} a^2(t), & f = f(t) \\ 0, & \text{otherwise.} \end{cases} \quad (6)$$

The Hilbert-Huang marginal spectrum $h(f)$ of the original signal $Y(t)$ can then be defined as the total energy distributed across the frequency space within a defined time period $[0, T]$. Mathematically, this can be expressed as shown below:

$$h(f) = \int_0^T H(f, t) dt. \quad (7)$$

By using Equations 6 & 7 we can obtain the Hilbert-Huang marginal spectrum for a univariate IMF. However, the application of the multivariate EMD results in multivariate IMF signals. In order to compute the Hilbert-Huang marginal spectrum of each IMF across all dimensions, we simply average $H_i(f, t)$ across $i = 1, \dots, k$ dimensions.

2.5 Relative power in each IMF

To understand how much each of the iEEG frequency bands contributed to a certain IMF, we first determined how much each dimension of the IMF contributed to the overall power of the IMF. To this end, we first obtained the mean power E_{ij} in each dimension j of every i -th IMF signal:

$$E_{ij} = \frac{\sum_{t=0}^T a_{ij}(t)^2}{T}, \quad (8)$$

where T is, as before, the number of time epochs, and $a_{ij}(t)$ is the instantaneous amplitude for the j -th dimension of i -th IMF signal at time point t . One of the main properties of MEMD is that multivariate signals are decomposed in multivariate IMF signal of the same dimensions, where all dimensions within an IMF share the same time-scale of fluctuation [21]. Hence, focusing on the mean power over time of each dimension within an IMF is a good indication of the power on a particular time scale. The relative contribution of each j -th dimension to the i -th IMF (or relative power) is then simply

$$R_{ij} = \frac{E_{ij}}{\sum_{j=1}^k E_{ij}}, \quad (9)$$

with k indicating the number of dimensions.

2.6 Spatial heterogeneity in each frequency band and component

In order to check if all channels contribute homogeneously to a NMF component in a particular frequency band, we used a measure of sparsity: the *Gini Index* or *Gini coefficient* [22]. Given a vector $\mathbf{x} = (x_1, x_2, \dots, x_N)$ sorted in ascending order such that $x_1 < x_2 < \dots < x_N$, the Gini Index can be derived using the following formula:

$$G(\mathbf{x}) = 1 - 2 \sum_{i=1}^N \frac{x_i}{\|\mathbf{x}\|_1} \left(\frac{N - i + \frac{1}{2}}{N} \right).$$

Gini Index is a measure for quantifying sparsity of a distribution. It takes values that ranges from 0 to 1. Values closer to 0 is an indication of low sparsity (homogeneity), while values closer to 1 corresponds to higher sparsity (heterogeneity).

Thus, we can derive a Gini index for each frequency band in each component of W . We will use this later, weighted by the relative power of particular IMFs to assess if all channels, or groups of channels contribute to certain IMFs.

2.7 IMF seizure distance

For each patient, we quantified the difference in IMF between pairs of seizures for each IMF. To achieve that, we first computed the product $W \times IMF_i(t)$ with IMF_i , representing the multi-dimensional i -th IMF ($k \times T$ matrix). The product yields the matrices X'_{IMF_i} for all $i = 1, \dots, M$ timescales. X'_{IMF_i} reconstructs the i -th IMF in the original space of all channels and frequency bands. For each X'_{IMF_i} , we computed a distance matrix based on the multivariate Euclidean distance of IMF values for each pair of seizures: $D_i(r, c) = \|X'_{IMF_i}(t_r) - X'_{IMF_i}(t_c)\|$, where t_r and t_c are the time epochs of the seizure pair's onset. Therefore, we obtain M IMF seizure distance matrices per patient, each representing the pairwise seizure distance for a specific IMF.

Note that any seizure-induced changes in the band power will only be present in a few epochs (as we use 30 s epochs). Therefore, the seizures are considered to influence only the fastest IMFs (highest-frequency fluctuations), while they have little effect on the slower IMFs. Supplementary Materials additionally shows that our main results reproduce for IMF seizure distances obtained from one epoch before the seizure onset epoch ($t_r - 1$ and $t_c - 1$).

2.8 Seizure dissimilarity

In our previous work, we introduced a quantitative measure of how dissimilar two seizures are within a patient [2]. Briefly, each epileptic seizure in a patient is analysed in terms of its evolution/pathway through the space of functional network dynamics. The pathways are then compared to each other using dynamic time warping, accounting for different seizures (or parts of seizures) that are very similar in dynamics but not in duration. The average distance between the warped seizures is then taken as the dissimilarity measure. For each patient, we can thus obtain a seizure dissimilarity matrix, which captures the pairwise dissimilarity between seizures of that given patient.

2.9 Association between seizure dissimilarity & IMF seizure distance

In the final part of our analysis, we will investigate if IMF seizure distances can explain seizure dissimilarity in each patient. This part of the analysis was performed for patients with more than 5 recorded seizures. We used a linear regression framework, where the seizure dissimilarity is the response variable and the IMF seizure distances are the explanatory variables. The observations are the upper/lower triangle of the matrices representing distances and dissimilarities of unique seizure pairs. We also included the temporal distances of seizures (how far apart in time each pair of seizures occurred) as an additional explanatory variable. All variables were standardised before including them in the model.

As a variable selection step for our analysis, we used LASSO [23], which is a sparse shrinkage method. Linear regression coefficients were calculated based on least squares, subject to the L_1 penalty. The LASSO also accounted for any collinearity issues between variables. As we were interested in detecting positive relationships between the response variable and the explanatory variables, we used a constrained positive LASSO, that is, coefficients are constrained to be non-negative. The shrinkage parameter λ for the LASSO model was selected using a 10-fold cross validation method from a range of values $\lambda = 10^{-3}, 10^{-2.95}, \dots, 10^{1.95}, 10^2$ (see Suppl. Fig.).

After selecting a small number of explanatory variables, an ordinary least squares regression was performed, for each patient, to obtain R^2 and 95% confidence intervals for the coefficients.

2.10 Statistical analysis

In order to assess if the “best” models selected for each patient could have been found by chance, we performed a permutation test for the adjusted R^2 .

In each permutation iteration, we first randomly shifted the seizure onset times within the recording period available. Then, for each iteration, we obtained new IMF seizure distance matrices and we performed the LASSO and linear regression, as described in the previous section, leaving the response variable unchanged. Finally, we calculated the adjusted R^2 for each iteration. Across all iterations, the adjusted R^2 values are used to form an estimation of the distribution of the test statistic used in the permutation test. P-values were then calculated as the percentage of adjusted

R^2 values that were larger in the permutation distribution. Statistical significance was determined based on a significance level of 1%.

We also performed an alternative permutation test, where we permuted the order of the seizures without permuting the seizure timing. The results are highly comparable and shown in detail in Supplementary Materials.

2.11 Data and code availability

The long-term iEEG recordings for all patients are available at <http://ieeg-swez.ethz.ch/> under the section “Long-term Dataset and Algorithms” [13].

Initial signal processing was performed using Matlab version 2019a and Matlab’s built-in functions. NMF and MEMD were implemented using the following publicly available functions:

- Non-negative matrix factorisation was conducted using the *NNSVD-LRC* function from <https://sites.google.com/site/nicolasgillis/code> [24].
- Multivariate EMD was applied using code from <http://www.commsp.ee.ic.ac.uk/~mandic/research/emd.htm> [25].

For the remainder of the analysis and the construction of all figures we used Python version 3.5. Either standard functions obtained from published libraries supported by Python were used or custom code written in Python. The main functions used in the analysis are listed below:

- **Hilbert transform:** `scipy.signal.hilbert`
- **Mantel test:** We used the `test` function available from <http://jwcarr.github.io/MantelTest/>[26].
- **LASSO:** `sklearn.linear_model.Lasso`
- **k-fold cross-validation:** `sklearn.model_selection.kFold`

For fitting **linear regression** models, we used the `lm` function from *stats* package implemented in RStudio version 1.1.463 using R version 3.6.3.

Our analysis code and data (post processing) can be found on TBC.

3 Results

We analysed the power of multi-channel iEEG signals in the five main frequency bands in terms of their underlying temporal fluctuations on various time-scales for 18 subjects with focal epilepsy. We specifically investigated if fluctuations on particular time scales were driven by particular iEEG frequency bands, or spatially localised activity. We then explored if these temporal fluctuations can explain how seizures change in their temporal evolution from one seizure to the next [2].

3.1 iEEG band power patterns fluctuate on different time scales

Following extraction of signal power in the main frequency bands ($\delta, \theta, \alpha, \beta, \gamma$) in 30 s sliding windows (no overlap) for each iEEG channel (Fig. 1a,b), we performed dimensionality reduction using non-negative matrix factorisation (NMF). NMF effectively groups channels and frequency bands together to form components (weights for each component are shown in matrix W , Fig. 1c). The

strength of these components at each time point is then given by the H matrix, which essentially yields a time series for each component (Fig. 1d). The original data matrix (Fig. 1b) can be approximately reconstructed from $W * H$. The set of time series in H show the fluctuations of particular band powers over time.

We then determined the different time-scales of fluctuations that were present in each NMF component of H for each patient using Multivariate Empirical Mode Decomposition (MEMD). Fig. 2a shows the MEMD results for a single NMF component in example patient ID06, yielding 16 Intrinsic Mode Functions (IMFs) in this case. Faster IMFs (e.g., IMF1, 2 and 3) are often thought to contain “noise”, and we investigate this in more detail in Supplementary Materials. However, for simplicity, we will retain all IMFs for the subsequent main results, and refer the reader to Supplementary Materials for a more detailed discussion.

Using the instantaneous frequency and amplitude through the Hilbert transform, we can obtain a representation of the marginal spectral densities of each IMF in each dimension/component. Fig. 2b shows the marginal spectral densities summed across all dimensions for each IMF (blue lines) for example patient ID06. Some distinct peaks are seen especially in the slower IMFs, e.g. IMF13 (at ≈ 1 cycle/day), IMF14 (at ≈ 0.3 cycle/day), IMF9 ≈ 8 cycles/day), IMF8 ≈ 15 cycles/day), etc. Note that EMD and MEMD as a method essentially acts as a dyadic filter bank [27, 28, 29], thus the dyadic pattern seen in the faster IMFs is not surprising.

Across all subjects, fluctuations with a 24h cycle are consistently seen (Fig. 2c). Fluctuations on other time scales can be subject-specific. For 12 out of 18 subjects (ID01, ID02, ID04, ID05, ID07, ID08, ID09, ID11, ID12, ID13, ID17 and ID18) the 24h cycle had the highest density. For 5 subjects (ID03, ID06, ID14, ID15 and ID16) the 24h cycle was slightly lower in density, as the highest density was linked to slower IMFs. For 1 subject (ID10) faster IMFs were marginally higher in density/energy followed by the 24h cycle IMF.

3.2 All iEEG main frequency bands contribute to the 24h IMF

Following the observation of a 24h cycle in all subjects, we want to assess the contribution of each iEEG main frequency band to this 24h fluctuation. To achieve this, we first determined the 24h IMF, which is IMF 13 in example patient ID06 (Fig. 3a). We then calculated the relative power in each dimension/component of the IMF. For example, in patient ID06, the majority of its power is concentrated in dimension/component 1 (54%). We also note that the 24h fluctuation does not follow the same phase in all dimensions/components of the IMF, potentially indicating the presence of multiple processes fluctuating on a 24h time scale (see Discussion for more details). For the sake of simplicity, we decided to assess the contribution of different frequency bands over all components/dimensions next.

From the dimensionality reduction step, we already know the weight of each iEEG frequency band for each channel (matrix W , see Fig. 3b). Thus, a summed weight can be obtained for each frequency band (across all channels). Finally, a sum weighted by the relative power in the IMF over all dimensions/components can then indicate the relative contribution of each frequency band to the IMF (Fig. 3c). For most subjects, δ band power contribution is slightly higher compared to the other frequency bands for the 24h cycle IMF. However, other frequency bands also contribute to the 24h cycle IMF in most patients. We also found that other IMFs have a relatively even contribution from all frequency bands in all patients (see online data TBC).

3.3 Groups of channels contribute to IMFs slower than 24h

Analogously to above, we also investigated the contribution of each channel (in each frequency band) to an IMF. Specifically, we investigated if the contributions were similar across all channels, or if the contributions were more heterogeneous. We used the weighted Gini index as a measure of spatial heterogeneity, where 0 (1) indicates a completely homogeneous (heterogeneous) contribution for each IMF. Fig. 4 shows the distribution of weighted Gini indices in the δ band across all patients and their IMFs grouped by the IMF dominant timescale of fluctuation. Results for other frequency bands are similar and shown in Supplementary Fig. Overall, the Gini indices are low for all IMFs, indicating that IMFs are not driven by one or few solitary channels. However, there is a clear tendency for slower IMFs (below 1 cycle per day) to display a higher Gini index, indicating that slower fluctuations may be driven by groups of channels.

In summary, we confirmed that the band power IMF fluctuations derived from MEMD are consistent across patients in terms of a circadian cycle, that the fluctuations are not solely dominated by one frequency band (which could indicate strong noise in a particular frequency band), and that the fluctuations are not dominated by one or few channels (another possible indication of strong noise in one channel).

3.4 Band power IMF fluctuations explain seizure dissimilarity in most patients

As the final part of our analysis, we investigated if these fluctuations on different time scales detected in the IMFs could explain our recent observation of changes in seizure properties over time in individual patients [2]. Particularly, we previously showed that EEG network dynamics change from one seizure to the next in every patient, and that these changes could be explained by hypothetical circadian or longer timescale modulators. Here, we explored if the patient-specific fluctuations detected by the IMFs explain changes in seizure dynamics.

For each IMF in each patient, we first determined their corresponding seizure IMF Euclidean distance matrix (Fig.5a,b). For example, in patient’s ID06 IMF 6, we calculated the Euclidean distance of every time point to the time point of the first seizure (Fig.5a) across all dimensions/components. By reading out all the Euclidean distances to all the other seizure time points, we obtained the first row of the seizure IMF Euclidean distance matrix (Fig.5b). The same process can be repeated for all other seizures in this patient. This distance matrix has dimensions of number of seizures by number of seizures and represents how different the IMF state is for each seizure pair.

By using the same techniques as in [2], we obtained a seizure dissimilarity matrix, which expresses how dissimilar each pair of seizure pathways are through the space of network dynamics (Fig.5c,d). The seizure dissimilarity matrix represents how each pair of seizures differ within a patient. By relating the seizure dissimilarity for each seizure pair to its corresponding IMF Euclidean distance, we can investigate if there is an association between the two. If the two measures are associated, as shown in the example in Fig.5(e), it indicates that the differences in seizure network dynamics can be explained by the IMF state differences.

To generalise this approach to all IMFs in a patient, we fitted a multiple linear regression model, where the seizure IMF distances are explanatory variables, and the seizure dissimilarity is the response variable (Fig.6a). We also included the temporal distance between seizures as an explanatory variable (i.e. how far apart in time each seizure pair occurred). The observations are pairs of seizures, and we fitted a model for each subject. To achieve adequate sample size, we only

included patients with more than 5 seizures. After LASSO variable selection and linear regression, the estimated regression coefficients for subject ID06 are shown in Fig.6(c). The strongest explanatory effect was seen in the slowest IMF (IMF16) followed by some faster IMFs (IMF3, 4, 5 and 6). For this particular subject, according to the model, 67.42% of the variability of seizure dissimilarity is explained by explanatory variables (i.e. Adjusted $R^2 = 0.6742$).

Out of all eight patients, six had an Adjusted R^2 around or above 0.6 (Fig.6d). Supplementary Fig. additionally shows that the adjusted R^2 values would have not occurred by chance, except for in ID10. Across all subjects, IMFs around, or slower than, 24h were part of the explanatory variables, except ID10 (Fig.6d). However, note that for patient ID10, the model had the lowest adjusted R^2 compared to all the other patients. Temporal distance between seizures remained as an explanatory variable in three subjects. Faster than 24h IMFs also tended to remain as explanatory variables in the models. Overall, a subject-specific combination of different fluctuations appears to provide a good explanation of seizure variability in most patients.

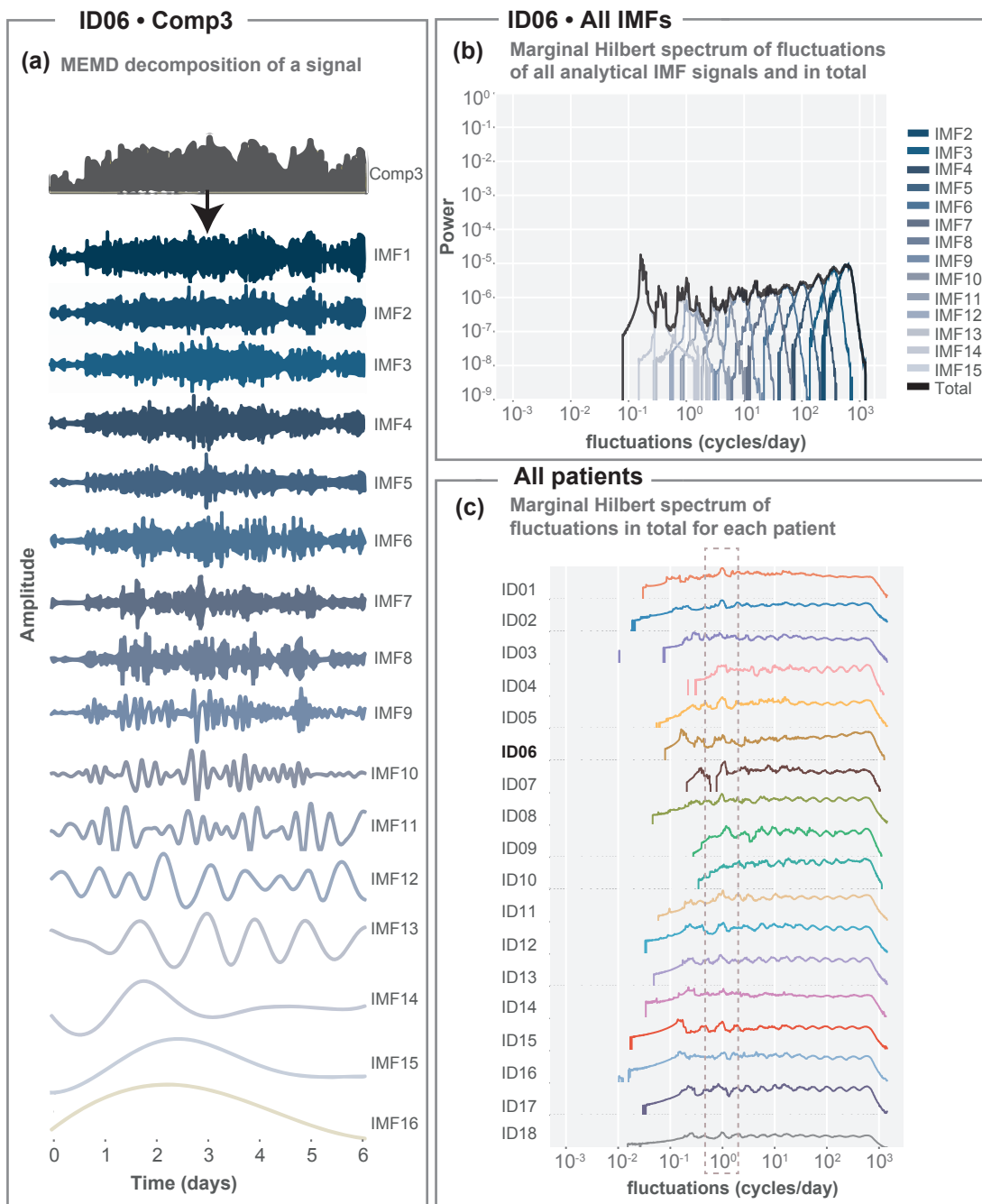


Figure 2: MEMD detects fluctuations on different time-scales across band power patterns (components) for each patient. (a) MEMD yields 16 IMFs in example patient ID06. Only one dimension of the IMF (corresponding to one NMF component) is shown for simplicity. IMFs are presented in descending order. (b) Marginal Hilbert spectrum of instantaneous frequencies for all IMFs (aggregated across all dimensions) in example patient ID06. The black line represents the Marginal Hilbert frequency spectrum across all IMFs; the last IMF was omitted for simplicity, as it contains the overall trend. (c) Marginal Hilbert frequency spectrum across all (but last) IMFs for each subject.

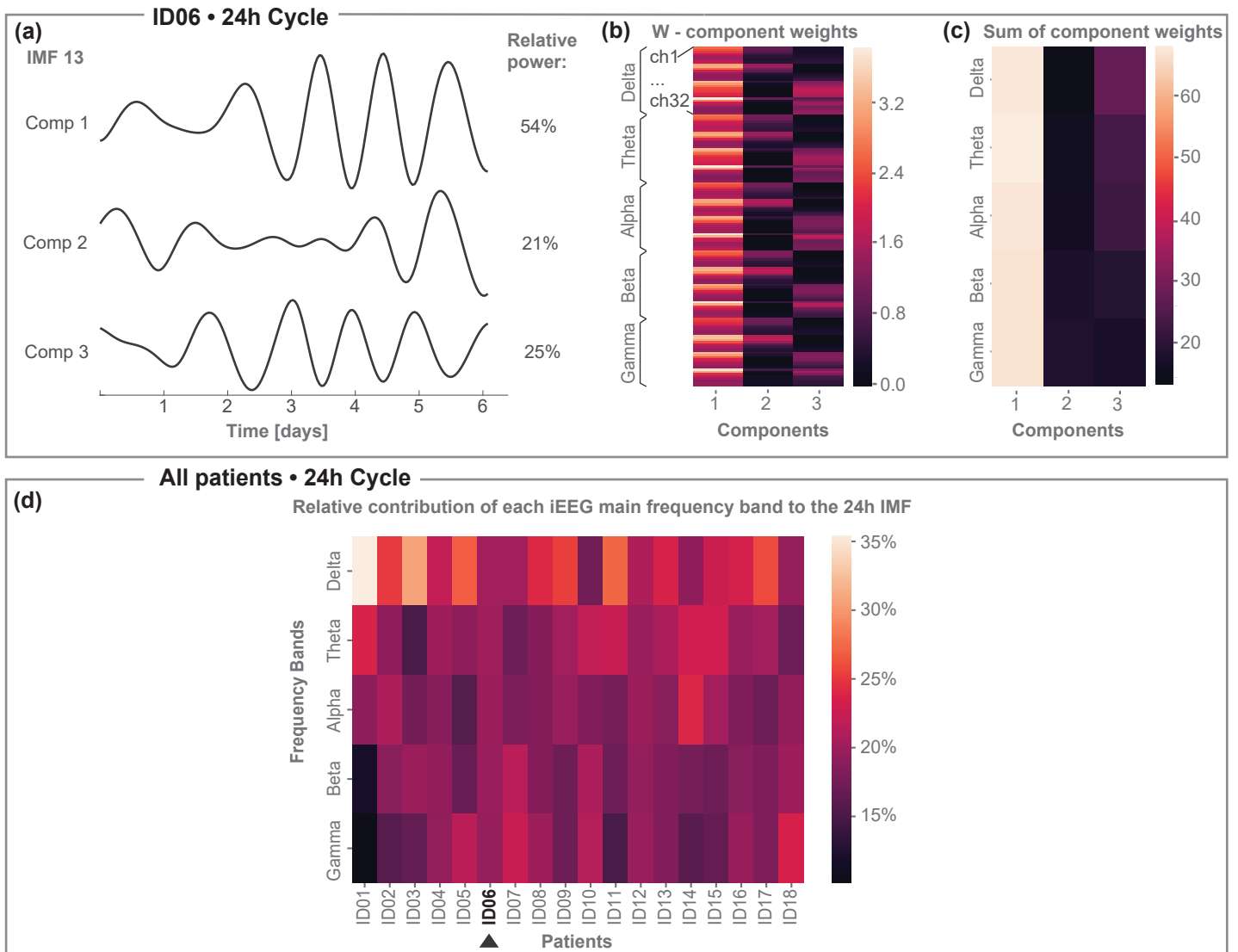


Figure 3: Contribution of iEEG main frequency bands to the 24h IMF. (a) IMF 13 in example patient ID06 shows fluctuations on the scale of 24h across all three dimensions/components. Component 1 shows the highest relative power in this IMF. (b) W component weight matrix (same as Fig. 1c). (c) The sum of the component weights across all channels within each frequency band. (d) Contribution of each iEEG main frequency band to the 24h IMF across all patients obtained by forming the sum over the matrix in (c) weighted by the relative power in (a). To be able to compare subjects to each other, each column here has been normalised to form a percentage contribution.

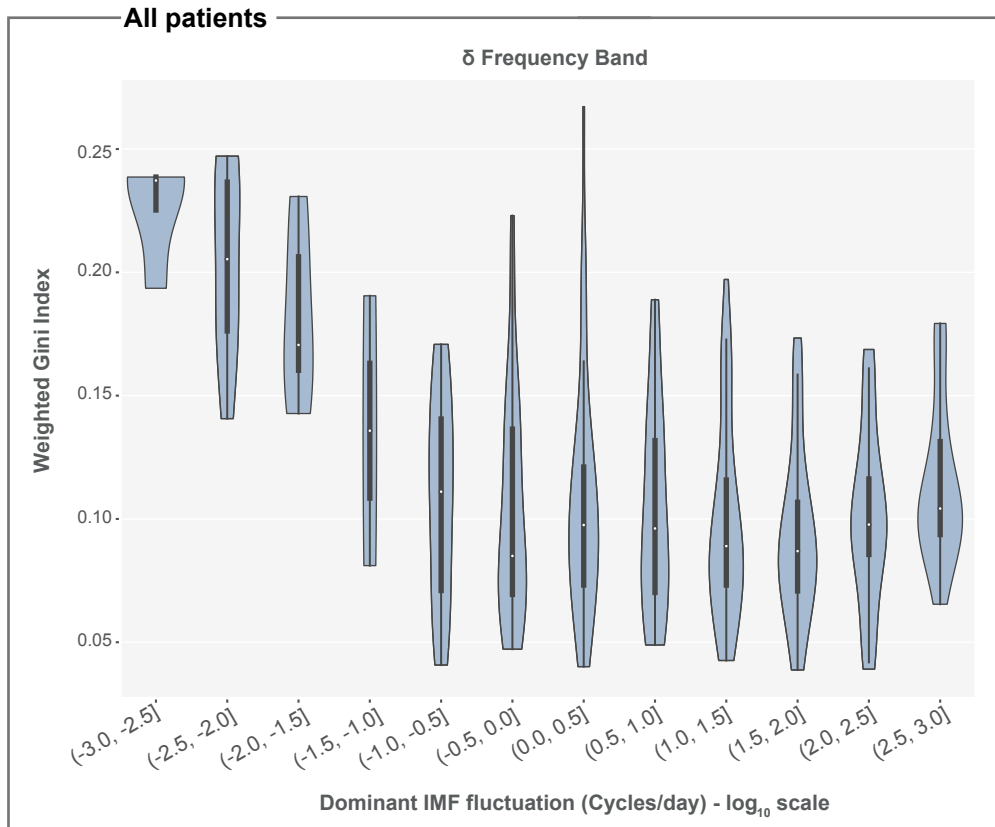


Figure 4: Weighted Gini Index for the δ frequency band across all patients. Across all patients, we grouped IMFs based on their dominant IMF fluctuation timescale and show the distribution of corresponding weighted Gini indices as a violin plot with enclosed box plot. The white dot represents the median, the thick grey bar represents the inter-quartile range.

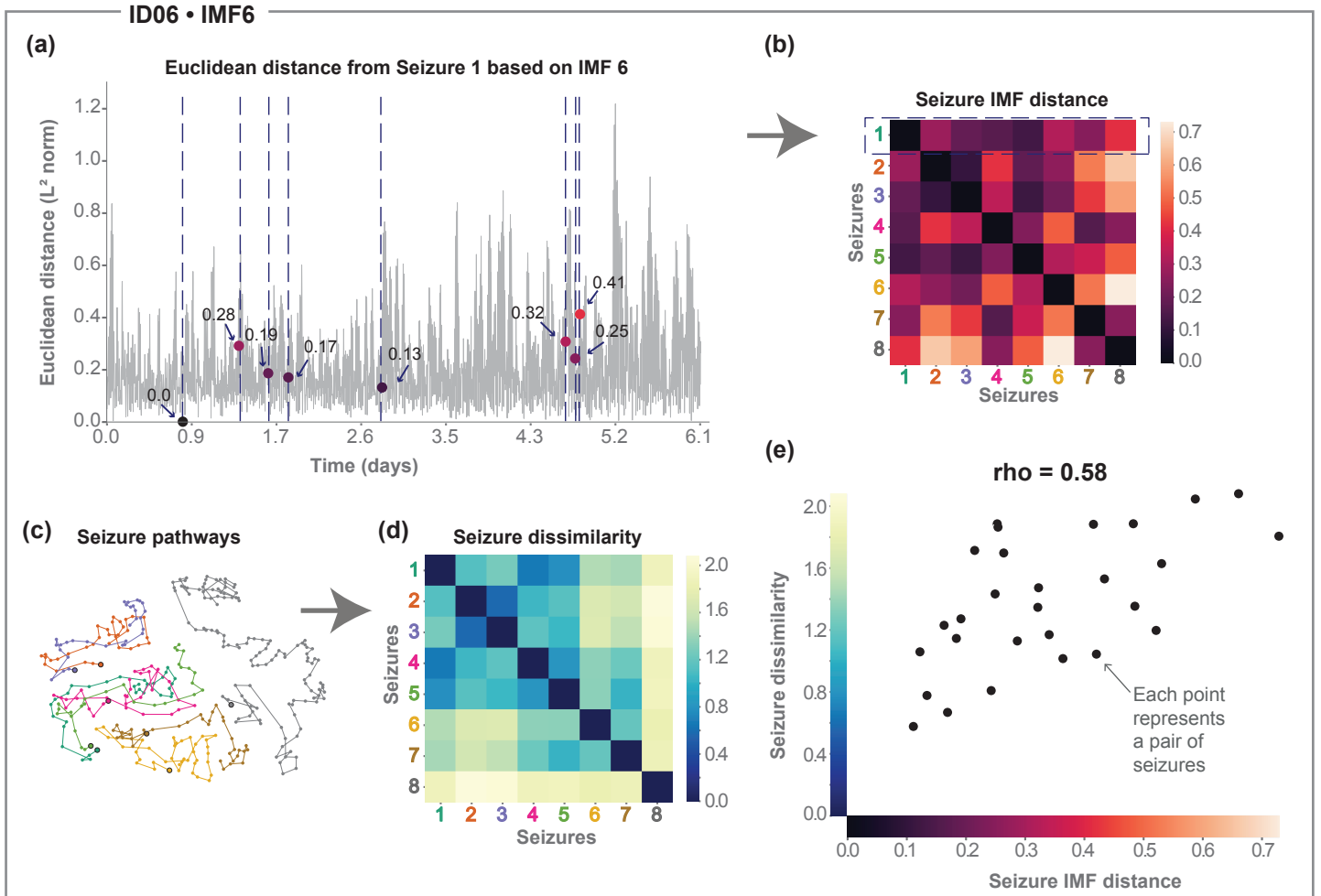


Figure 5: Relating seizure dissimilarity and IMF seizure distance. Throughout this figure we use example subject ID06 and IMF 6. (a) Euclidean distance of all time points to the first seizure in terms of IMF 6. Blue dashed vertical lines indicate seizure timing. Dots mark the value of the IMF distance to the first seizure and colours of dots correspond to the colour scale in (b). (b) Seizure IMF distance matrix for IMF 6. The first row is a representation of the data in (a). (c) Functional network evolution of all seizures projected into 2D space using multidimensional scaling (MDS) for visualisation of seizure pathways (see [2] for details). Similar seizures tend to be placed closer together in this projection. Seizures are displayed with distinct colours to distinguish seizure events. The starting points of seizures are marked with a black outline circle. (d) Seizure dissimilarity matrix, capturing the differences in seizure pathways over time between each pair of seizures. (e) Scatter plot of seizure dissimilarity and the seizure IMF distance (Spearman's correlation, $\rho = 0.58$, $p=0.04$). P-value obtained from the Mantel test, and it is FDR corrected for all IMFs in all patients.

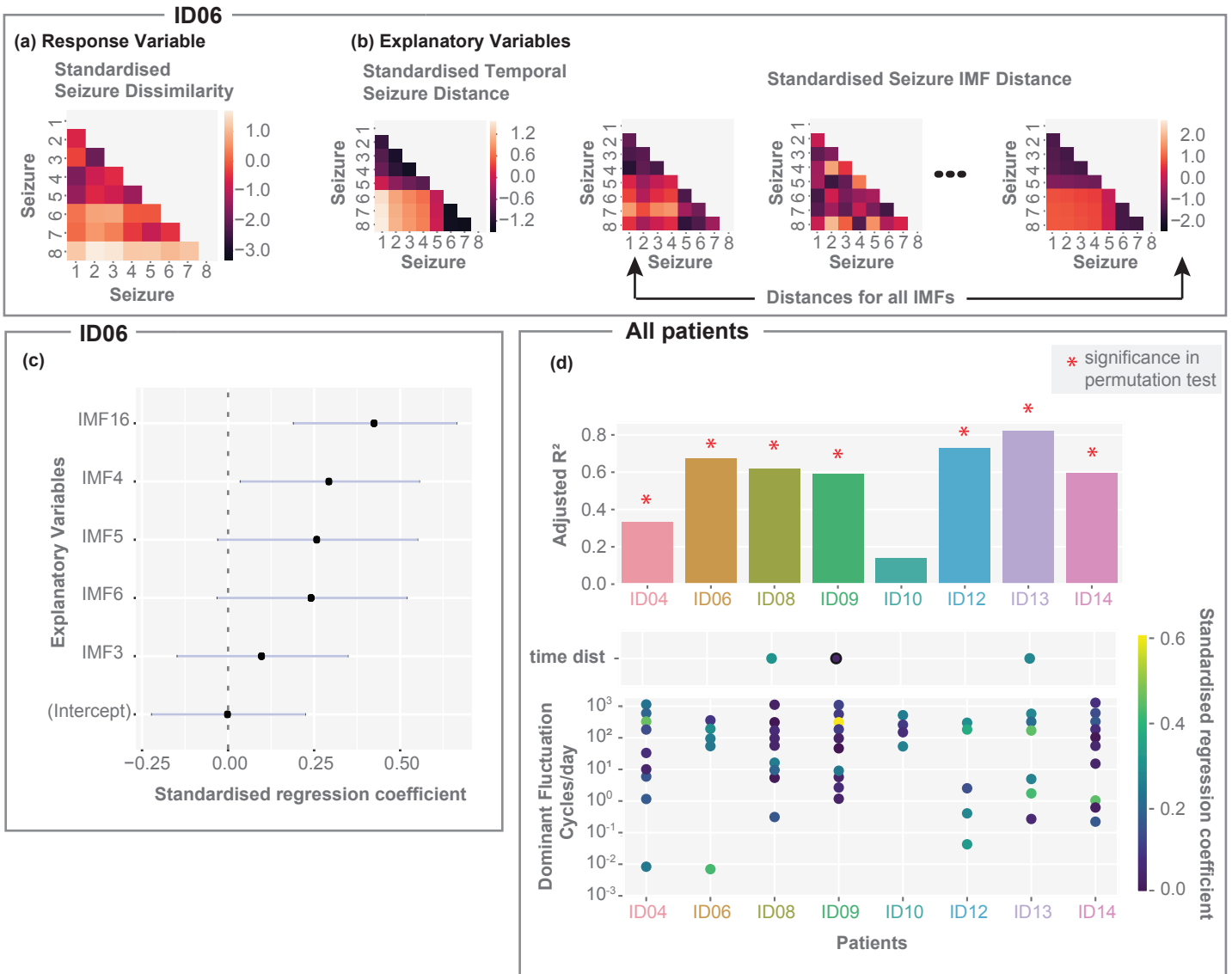


Figure 6: IMF seizure distances can explain seizure dissimilarity in most patients. (a) Standardised seizure dissimilarity matrix (response variable). Only the lower triangle of the symmetric matrix is shown, where each entry serves as an observation. (b) The matrix on the left shows the standardised temporal seizure distance. Each entry corresponds to the absolute time difference between seizures. The remaining matrices are standardised seizure IMF distance matrices. (c) Coefficient estimates (black dots), based on ordinary least squares regression for ID06, with lines indicating 95% confidence intervals. Only five explanatory variables (IMFs) were left after performing variable selection based on constrained LASSO. (d) Summary across patients based on OLS models with explanatory variables obtained by the constrained LASSO. Top: Bar chart of the Adjusted R^2 . Red stars indicate p -values ≤ 0.05 in permutation tests. Bottom: Dot plot indicating the OLS coefficient estimates for the time distance (when this variable remained in the model) together with OLS coefficient estimates at the corresponding value of dominant IMF fluctuation timescale for each subject.

4 Discussion

We performed a quantitative analysis of multi-channel continuous long-term iEEG recordings from 18 focal epilepsy patients. We extracted the band power time series in each channel and identified the temporal fluctuations on various time-scales. Consistent with other studies, we observed the presence of a circadian rhythm in band power fluctuations across all subjects. Fluctuations on other time scales were also apparent, but varied between patients, suggesting that various patient-specific fluctuations coexist. In most patients, these patient-specific fluctuations on different timescales provided a good explanation for the patient’s seizure dissimilarity (a measure that was previously proposed [2] to assess how much the seizure dynamics changed from one seizure to the next within each patient).

Fluctuations on various time-scales of the continuous EEG have been reported in several studies using prolonged iEEG recordings. The prevalence of a strong circadian rhythm in EEG patterns is well known since 1969 [30, 31, 32, 33]. Weaker ultradian rhythms have also been reported in long-term EEG band power during daytime wakefulness in healthy subjects [34, 35]. For example, ultradian modulations are reported to occur with a cycle of 2 and 4 hours in the 9-11 Hz and 11-13 Hz frequency bands, respectively [34]. Using a functional connectivity measure of EEG, [8] also reported ultradian fluctuations additional to a strong circadian rhythm. Recently, patient-specific multidien (multi-day) rhythms have been detected in the rate of interictal epileptiform activity in epilepsy patients [12, 10]. Similarly, daily and longer cycles were shown in the variance and autocorrelation of EEG signals [36]. Our observations are in agreement with these previous findings. Apart from the 24h cycle that was apparent in all subjects, we observed fluctuations on ultradian and infradian time-scales that were subject-specific.

We additionally made two observations about these fluctuations on different time scales. First, we saw that different frequency bands appear to contribute to a similar degree to the circadian fluctuation of iEEG band power, although subject-specific patterns of contribution were also noted. However, our analysis was performed on the multidimensional IMFs (across all dimensions/components) corresponding to the circadian fluctuation in each patient. The different components of the IMF were not identical (see e.g. Fig. 3a), indicating that different circadian fluctuations (with different phases) exist in each patient, as has been reported before [33]. Future work may wish to investigate the different dimensions of the IMF separately in terms of what frequency bands contribute to them, and to relate them to other physiological variables such as body temperature or plasma melatonin [33].

The second observation we made was that slower (infradian) fluctuations tended to arise from groups of channels, whereas faster (circadian and ultradian) fluctuations tended to arise as a more equal contribution from all channels. Again, similar to our first observation, we also performed our analysis over all dimensions of the IMFs, not distinguishing between IMF components. Individual components of IMFs may well (and do) have spatially heterogeneous contributors. To fully uncover the spatial and frequency band contributions to each component of each IMF, we suggest that future work performs an iterative dimensionality reduction and empirical mode decomposition to optimally find components and component contributions for each IMF.

Our main goal was to investigate if fluctuations in long-term iEEG band power explain seizure dissimilarity within each patient. Seizure dissimilarity is a measure that was proposed to assess how different any pair of seizures are in a given patient in terms of their seizure evolution and dynamics. Previous work has also shown that seizure dissimilarity was well-explained by processes incorporating Gaussian noise, circadian and/or slower timescales changes in most patients [2]. In agreement, we found that circadian or infradian fluctuations contributed strongly in most patients

in explaining seizure dissimilarity. Interestingly, we also found many faster (ultradian) fluctuations as explanatory variables in most patients. These could be contributing explanatory power through what previously was modelled as noise. With larger datasets using many more seizures recorded over a longer period, future work should investigate ultradian contributions carefully and assess if noise would perform as well as the cumulative ultradian contributions.

We also wish to point out that the band power fluctuations did not account for all the variability of seizure dissimilarity in most patients. The highest R^2 was around 0.8 and the unexplained variability based on the models suggests that there are additional factors that impact seizure dynamics. One such factor may be the anti-epileptic drug (AED) level at any given time. Patients undergoing such prolonged iEEG monitoring often undergo AED withdrawal as part of the clinical evaluation. It is also well-known that AED changes and withdrawal can change the severity and dynamics of seizures. For example, bilateral tonic-clonic seizures are more prevalent when AED levels are reduced [37]. We were unable to include this information in the current study, but future studies may wish to investigate AED levels as additional potential explanatory variables for seizure dissimilarity.

In a more general context, our work is another contribution to the wider literature of explaining ictal features from interictal EEG features, or hypothesised circadian/infradian rhythms. Most notably, the ictal feature of interest is often the seizure timing (when a seizure occurs). For example, studies have established that there is often a (subject-specific) relationship between fluctuations of interictal EEG features and the timing of ictal events [12, 10, 8]. A number of studies also demonstrated that seizure occurrence is underpinned by a circadian/infradian rhythms [12, 10, 38, 39, 31]. Interestingly, we found no evidence of an association between band power fluctuations of the interictal EEG and seizure occurrence (data not shown). Seizures were not statistically more likely to occur during particular phases of particular IMFs in most patients in our data set. This is in agreement with a previous study [8] that reported functional network fluctuations, rather than band power fluctuations, to be more predictive of seizure timing. Therefore, future work should investigate temporal fluctuations in a range of EEG features, such as band power, functional connectivity [8], high frequency oscillations [9], variance and autocorrelation [36], just to name a few. Apart from seizure timing, our work has shown that these fluctuations on different timescales of the interictal EEG also explain other features of the seizures (in our case seizure dissimilarity). Future work should explore this avenue further to elucidate the exact processes and timescales that modulate or dictate the various aspects of a seizure.

A variety of possible factors, both external and internal, could explain the observations above of interictal EEG fluctuations on different time scales, and correlated changes in seizure features. External factors may be environmental processes such as lower atmospheric pressure, high air humidity and temperature [40] or processes related to nutrition, such as caffeine [41].

Internal factors, linked to external factors, include emotional/physical stress [42], low quality of sleep [43], and fatigue [44]. Other internal factors include hormonal rhythms (e.g. menstrual cycles) [45, 46] and circadian rhythms [47]. Seizure frequency, seizure dynamics, interictal epileptic phenomena (e.g. spikes, bursts, HFOs) and general interictal EEG patterns all might be affected by these time-varying factors [48, 49]. However, the exact relationship between modulators and epileptic processes remains to be explored in future.

In conclusion, seizure occurrence/timing may not be the only aspect of a seizure that is correlated with fluctuating interictal EEG features. Our work has shown that the EEG evolution and dynamics during a seizure may be modulated by such interictal fluctuations on infradian, circadian, and ultradian time-scales. The implication is that EEG fluctuations on different timescales may predict seizure dynamics. Due to the tremendous impact epilepsy has on the quality of a patient's

life, it is necessary to provide predictions of various seizure features based on the patient’s needs, including seizure severity. Furthermore, if interictal fluctuations can be manipulated, then they may also causally alter seizure dynamics. As a novel therapeutic approach, seizures may then be rendered less severe as a consequence.

References

- [1] C. E. Stafstrom and L. Carmant, “Seizures and Epilepsy: An Overview for Neuroscientists,” *Cold Spring Harb Perspect Med*, vol. 5, p. a022426, June 2015.
- [2] G. M. Schroeder, B. Diehl, F. A. Chowdhury, J. S. Duncan, J. d. Tisi, A. J. Trevelyan, R. Forsyth, A. Jackson, P. N. Taylor, and Y. Wang, “Seizure pathways change on circadian and slower timescales in individual patients with focal epilepsy,” *PNAS*, May 2020.
- [3] V. K. Jirsa, W. C. Stacey, P. P. Quilichini, A. I. Ivanov, and C. Bernard, “On the nature of seizure dynamics,” *Brain*, vol. 137, pp. 2210–2230, Aug. 2014.
- [4] M. L. Saggio, D. Crisp, J. Scott, P. J. Karoly, L. Kuhlmann, M. Nakatani, T. Murai, M. DümpeImann, A. Schulze-Bonhage, A. Ikeda, M. Cook, S. V. Gliske, J. Lin, C. Bernard, V. Jirsa, and W. Stacey, “Epidynamics characterize and navigate the map of seizure dynamics,” *bioRxiv*, p. 2020.02.08.940072, Feb. 2020.
- [5] B. Oken and K. Chiappa, “Short-term variability in EEG frequency analysis,” *Electroencephalography and Clinical Neurophysiology*, vol. 69, pp. 191–198, Mar. 1988.
- [6] C. Geier, K. Lehnertz, and S. Bialonski, “Time-dependent degree-degree correlations in epileptic brain networks: from assortative to dissortative mixing,” *Front. Hum. Neurosci.*, vol. 9, 2015.
- [7] C. Geier and K. Lehnertz, “Long-term variability of importance of brain regions in evolving epileptic brain networks,” *Chaos*, vol. 27, p. 043112, Apr. 2017.
- [8] G. D. Mitsis, M. N. Anastasiadou, M. Christodoulakis, E. S. Papathanasiou, S. S. Papacostas, and A. Hadjipapas, “Functional brain networks of patients with epilepsy exhibit pronounced multiscale periodicities, which correlate with seizure onset,” *Human Brain Mapping*, vol. 41, no. 8, pp. 2059–2076, 2020.
- [9] S. V. Gliske, Z. T. Irwin, C. Chestek, G. L. Hegeman, B. Brinkmann, O. Sagher, H. J. L. Garton, G. A. Worrell, and W. C. Stacey, “Variability in the location of high frequency oscillations during prolonged intracranial EEG recordings,” *Nat Commun*, vol. 9, p. 2155, Dec. 2018.
- [10] P. J. Karoly, D. R. Freestone, R. Boston, D. B. Grayden, D. Himes, K. Leyde, U. Seneviratne, S. Berkovic, T. O’Brien, and M. J. Cook, “Interictal spikes and epileptic seizures: their relationship and underlying rhythmicity,” *Brain*, vol. 139, pp. 1066–1078, Apr. 2016.
- [11] E. C. Conrad, S. B. Tomlinson, J. N. Wong, K. F. Oechsel, R. T. Shinohara, B. Litt, K. A. Davis, and E. D. Marsh, “Spatial distribution of interictal spikes fluctuates over time and localizes seizure onset,” *Brain*, vol. 143, pp. 554–569, Feb. 2020.

- [12] M. O. Baud, J. K. Kleen, E. A. Mirro, J. C. Andrechak, D. King-Stephens, E. F. Chang, and V. R. Rao, “Multi-day rhythms modulate seizure risk in epilepsy,” *Nature Communications*, vol. 9, p. 88, Jan. 2018.
- [13] A. Burrello, L. Cavigelli, K. Schindler, L. Benini, and A. Rahimi, “Laelaps: An Energy-Efficient Seizure Detection Algorithm from Long-term Human iEEG Recordings without False Alarms,” in *2019 Design, Automation & Test in Europe Conference & Exhibition (DATE)*, (Florence, Italy), pp. 752–757, IEEE, Mar. 2019.
- [14] D. D. Lee and H. S. Seung, “Learning the parts of objects by non-negative matrix factorization,” *Nature*, vol. 401, pp. 788–791, Oct. 1999.
- [15] S. M. Atif, S. Qazi, and N. Gillis, “Improved SVD-based initialization for nonnegative matrix factorization using low-rank correction,” *Pattern Recognition Letters*, vol. 122, pp. 53–59, May 2019.
- [16] N. E. Huang, Z. Shen, S. R. Long, M. C. Wu, H. H. Shih, Q. Zheng, N.-C. Yen, C. C. Tung, and H. H. Liu, “The empirical mode decomposition and the Hilbert spectrum for nonlinear and non-stationary time series analysis,” *Proc. R. Soc. Lond. A*, vol. 454, pp. 903–995, Mar. 1998.
- [17] N. E. Huang, M.-L. C. Wu, S. R. Long, S. S. P. Shen, W. Qu, P. Gloersen, and K. L. Fan, “A Confidence Limit for the Empirical Mode Decomposition and Hilbert Spectral Analysis,” *Proceedings: Mathematical, Physical and Engineering Sciences*, vol. 459, no. 2037, pp. 2317–2345, 2003.
- [18] A. Y. Kaplan, A. A. Fingelkurts, A. A. Fingelkurts, S. V. Borisov, and B. S. Darkhovsky, “Nonstationary nature of the brain activity as revealed by EEG/MEG: Methodological, practical and conceptual challenges,” *Signal Processing*, vol. 85, pp. 2190–2212, Nov. 2005.
- [19] A. A. Fingelkurts and A. A. Fingelkurts, “Operational Architectonics of the Human Brain Biopotential Field: Towards Solving the Mind-Brain Problem,” *Brain and Mind*, vol. 2, pp. 261–296, Dec. 2001.
- [20] G. Rilling, P. Flandrin, P. Goncalves, and J. M. Lilly, “Bivariate Empirical Mode Decomposition,” *IEEE Signal Processing Letters*, vol. 14, pp. 936–939, Dec. 2007.
- [21] Y. Lv, R. Yuan, and G. Song, “Multivariate empirical mode decomposition and its application to fault diagnosis of rolling bearing,” *Mechanical Systems and Signal Processing*, vol. 81, pp. 219–234, Dec. 2016.
- [22] N. P. Hurley and S. T. Rickard, “Comparing Measures of Sparsity,” *arXiv:0811.4706 [cs, math]*, Apr. 2009. arXiv: 0811.4706.
- [23] R. Tibshirani, “Regression Shrinkage and Selection via the Lasso,” *Journal of the Royal Statistical Society. Series B (Methodological)*, vol. 58, no. 1, pp. 267–288, 1996.
- [24] A. M. Syed, S. Qazi, and N. Gillis, “Improved SVD-based Initialization for Nonnegative Matrix Factorization using Low-Rank Correction,” *Pattern Recognition Letters*, vol. 122, pp. 53–59, May 2019. arXiv: 1807.04020.

- [25] N. Rehman and D. P. Mandic, “Multivariate empirical mode decomposition,” *Proc. R. Soc. A.*, vol. 466, pp. 1291–1302, May 2010.
- [26] N. Mantel, “The Detection of Disease Clustering and a Generalized Regression Approach,” *Cancer Res*, vol. 27, pp. 209–220, Feb. 1967.
- [27] Z. Wu and N. E. Huang, “A study of the characteristics of white noise using the empirical mode decomposition method,” *Proc. R. Soc. Lond. A*, vol. 460, pp. 1597–1611, June 2004.
- [28] P. Flandrin, G. Rilling, and P. Goncalves, “Empirical mode decomposition as a filter bank,” *IEEE Signal Processing Letters*, vol. 11, pp. 112–114, Feb. 2004.
- [29] N. ur Rehman and D. P. Mandic, “Filter Bank Property of Multivariate Empirical Mode Decomposition,” *IEEE Trans. Signal Process.*, vol. 59, pp. 2421–2426, May 2011.
- [30] H. Scheich, “Interval histograms and periodic diurnal changes of human alpha rhythms,” *Electroencephalogr Clin Neurophysiol*, vol. 26, p. 442, Apr. 1969.
- [31] D. C. Spencer, F. T. Sun, S. N. Brown, B. C. Jobst, N. B. Fountain, V. S. S. Wong, E. A. Mirro, and M. Quigg, “Circadian and ultradian patterns of epileptiform discharges differ by seizure-onset location during long-term ambulatory intracranial monitoring,” *Epilepsia*, vol. 57, pp. 1495–1502, Sept. 2016.
- [32] M. K. Smyk and G. van Luijtelaar, “Circadian Rhythms and Epilepsy: A Suitable Case for Absence Epilepsy,” *Front. Neurol.*, vol. 11, 2020.
- [33] D. Aeschbach, J. R. Matthews, T. T. Postolache, M. A. Jackson, H. A. Giesen, and T. A. Wehr, “Two circadian rhythms in the human electroencephalogram during wakefulness,” *American Journal of Physiology-Regulatory, Integrative and Comparative Physiology*, vol. 277, pp. R1771–R1779, Dec. 1999.
- [34] D. A. Kaiser, “Ultradian and Circadian Effects in Electroencephalography Activity,” p. 4, 2008.
- [35] F. Chapotot, C. Jouny, A. Muzet, A. Buguet, and G. Brandenberger, “High frequency waking EEG: reflection of a slow ultradian rhythm in daytime arousal,” *NeuroReport*, vol. 11, pp. 2223–2227, July 2000.
- [36] M. I. Maturana, C. Meisel, K. Dell, P. J. Karoly, W. D’Souza, D. B. Grayden, A. N. Burkitt, P. Jiruska, J. Kudlacek, J. Hlinka, M. J. Cook, L. Kuhlmann, and D. R. Freestone, “Critical slowing down as a biomarker for seizure susceptibility,” *Nat Commun*, vol. 11, May 2020.
- [37] M. C. Pensel, M. Schnuerch, C. E. Elger, and R. Surges, “Predictors of focal to bilateral tonic-clonic seizures during long-term video-EEG monitoring,” *Epilepsia*, vol. 61, no. 3, pp. 489–497, 2020.
- [38] P. J. Karoly, H. Ung, D. B. Grayden, L. Kuhlmann, K. Leyde, M. J. Cook, and D. R. Freestone, “The circadian profile of epilepsy improves seizure forecasting,” *Brain*, vol. 140, pp. 2169–2182, Aug. 2017.

- [39] P. J. Karoly, D. M. Goldenholz, D. R. Freestone, R. E. Moss, D. B. Grayden, W. H. Theodore, and M. J. Cook, “Circadian and circaseptan rhythms in human epilepsy: a retrospective cohort study,” *The Lancet Neurology*, vol. 17, pp. 977–985, Nov. 2018.
- [40] F. Rakers, M. Walther, R. Schiffner, S. Rupprecht, M. Rasche, M. Kockler, O. W. Witte, P. Schlattmann, and M. Schwab, “Weather as a risk factor for epileptic seizures: A case-crossover study,” *Epilepsia*, vol. 58, no. 7, pp. 1287–1295, 2017.
- [41] R. R. van Koert, P. R. Bauer, I. Schuitema, J. W. Sander, and G. H. Visser, “Caffeine and seizures: A systematic review and quantitative analysis,” *Epilepsy Behav*, vol. 80, pp. 37–47, 2018.
- [42] E. Baldin, W. A. Hauser, A. Pack, and D. C. Hesdorffer, “Stress is associated with an increased risk of recurrent seizures in adults,” *Epilepsia*, vol. 58, no. 6, pp. 1037–1046, 2017.
- [43] C. W. Bazil and T. S. Walczak, “Effects of Sleep and Sleep Stage on Epileptic and Nonepileptic Seizures,” *Epilepsia*, vol. 38, no. 1, pp. 56–62, 1997.
- [44] O.-Y. Kwon, H. S. Ahn, and H. J. Kim, “Fatigue in epilepsy: A systematic review and meta-analysis,” *Seizure*, vol. 45, pp. 151–159, Feb. 2017.
- [45] J. Bauer, “Interactions Between Hormones and Epilepsy in Female Patients,” *Epilepsia*, vol. 42, no. s3, pp. 20–22, 2001.
- [46] E. Taubøll, L. Sveberg, and S. Svalheim, “Interactions between hormones and epilepsy,” *Seizure*, vol. 28, pp. 3–11, May 2015.
- [47] S. Khan, L. Nobili, R. Khatami, T. Loddenkemper, C. Cajochen, D.-J. Dijk, and S. H. Eriksson, “Circadian rhythm and epilepsy,” *The Lancet Neurology*, vol. 17, pp. 1098–1108, Dec. 2018.
- [48] D. R. Freestone, P. J. Karoly, and M. J. Cook, “A forward-looking review of seizure prediction:,” *Current Opinion in Neurology*, vol. 30, pp. 167–173, Apr. 2017.
- [49] R. A. B. Badawy, D. R. Freestone, A. Lai, and M. J. Cook, “Epilepsy: Ever-changing states of cortical excitability,” *Neuroscience*, vol. 222, pp. 89–99, Oct. 2012.